CERN SPSC 90-1
SPSC P248
December 22 1989

Proposal for the Study of Spin Effects in pp and $\bar{p}p$ Interactions Using a Polarized Atomic Hydrogen Beam Target

Bologna-CERN-Lausanne-Michigan-Milano-Rockefeller-Trieste-Udine

Bologna	G. Valenti
CERN	G. Ballocchi, L. Camilleri, W. Kubischta,
Lausanne	C. Joseph, P. Oberson, J. L. Pagès, J.P. Perroud,
	D. Ruegger, L. Studer, M.T. Tran, M. Werlen,
Michigan	D. Hubbard, O.E. Overseth, G.R. Snow,
Milan	L. Dick,
Rockefeller	P.T. Cox, P. Giacomelli, A. Vacchi,
Trieste	A. Penzo,
Udine	G. Paoletta.

GENEVA

1989

1. INTRODUCTION

The original proposal [1] for a gas jet target in the SPS tunnel was based on a polarized atomic hydrogen jet. It was designed to study the spin dependence of elastic scattering and of the inclusive production of π^o and Λ in pp interactions by using the jet during fixed target operation of the SPS. When the $\bar{p}p$ collider was approved it became possible to study, with high statistics, differences between pp and $\bar{p}p$ collisions in the production of π^o, η, direct photons, electron pairs and photon pairs as well as in elastic scattering. In all the above reactions the largest differences are expected at the highest transverse momenta, p_T, and at the highest invariant masses. Since this is also where cross sections are smallest, it was of interest to use as dense a jet as possible. It was therefore decided to use a high density molecular jet instead of the polarized atomic hydrogen jet. A proposal to study the above high transverse momentum reactions using a molecular jet was submitted [2] to the SPSC in 1980 and approved as experiment UA6.

After an initial short run in 1984, UA6 collected data in the $\bar{p}p$ mode in 1985 and in the pp mode in 1986. Results have been published on π^o cross sections [3] (Fig.1), on the η/π ratio [3] (Fig.2), on direct photon cross sections [4] (Fig.3), on small t elastic scattering [5] (Fig.4), and on electron pairs (J/ψ) [6] (Fig.5).

The approval of ACOL, which has yielded a tenfold increase in the $\bar{p}$ intensity led to the approval of a UA6 upgrade [7]. The upgraded UA6 collected pp data in 1987 and 1988 and $\bar{p}p$ data in 1989.

Although polarization has been measured in hadronic reactions at low energies, it was expected not so long ago that at high energies spin effects in hadronic collisions would disappear. This behaviour was indeed evident in elastic scattering where polarization effects were found to diminish with increased energy. The dogma was that at high energies and modest p_T hadron collisions were so complicated and involved so many inelastic channels that no coherent interference of amplitudes and hence no spin effects could result. However the physics of spin in high energy hadronic reactions has continued to produce unexpected results. A few examples are :

- at large t asymmetries continued to be observed in elastic scattering [8].

- the discovery that inclusively produced Λ are polarized, that their polarization increases with transverse momentum [9] and that it is present even at the highest energies at which it has been measured [10] ($\sqrt{s}$ of 53 GeV).
- the observation of single spin asymmetries [11,15] in the inclusive production of protons and pions using polarized targets or beams
- the recent and unexpected EMC result [16] shows our lack of understanding of the spin structure of the proton.

A convincing theoretical explanation of these large spin effects has yet to come. Various phenomenological models have been proposed for Λ polarization [27,28]. None are general enough to successfully explain more than a few results at best. However, at low transverse momentum ($\leq$ 3 GeV/c), where most of the data lie, QCD can say little or nothing as perturbative methods do not apply. It is therefore of fundamental importance to measure these effects at the highest transverse momenta and highest energies where perturbative QCD calculations can be performed.

The UA6 collaboration, joined by some new groups, is therefore proposing to develop a polarized atomic beam and install it in place of its molecular jet in the SPS tunnel in 1991. The physics aim is to make a comprehensive measurement of the single spin asymmetries in inclusive high p_T production of direct photons, π^o, η, ω^o , J/ψ and Λ in both pp and $\bar{p}p$ interactions at 315 GeV/c incident momentum. Furthermore, the measurement is to be made with a pure hydrogen target with a high degree of polarization (>90%) thus minimizing corrections to the data and therefore reducing systematic errors. It is to be hoped that the measurement of single spin asymmetries for a variety of secondaries and with two different incident particles will give clues to the origin of such asymmetries.

2. PHYSICS GOALS

In an elastic or inelastic interaction, the direction of polarization of either the target or the beam defines a plane orthogonal to this direction (Fig.6). In an optimum measurement of the transverse asymmetry A_n, in single particle production, one compares the number N_+ of particles scattered in this plane into a detector with the number N_- of particles scattered into the same detector but with a reversed direction of polarization. A_n is then defined as

$$A_n = \frac{1}{P} \frac{N_+ - N_-}{N_+ + N_-}$$

The error in the asymmetry is given by

$$\delta A_n = \frac{1 - A_n P}{P} \sqrt{\frac{1 + 2\alpha}{L\sigma T}}$$

where:

L = luminosity,
σ = spin averaged cross section per nucleon,
T = running time,
α = background/signal ratio averaged over the two spin orientations
P = target (or beam) polarization

It is conventional to quote a figure of merit for a single spin asymmetry measurement facility as

$$F = P^2 L$$

2.1 Inclusive production of γ, π^o, η, ω^o, J/ψ

Non-zero asymmetries have been observed in the inclusive production of :

- protons using a polarized incident proton beam of 11.75 GeV/c [11] and of 13.5 and 18.5 GeV/c [12].

- negative and positive pions using a polarized incident proton beam of 11.75 GeV/c [11] and of 13.5 and 18.5 GeV/c [12] (Fig.7).
- π^0 mesons using an incident proton beam of 24 GeV/c on a polarized target [13] (Fig.8).
- π^0 mesons using an incident π^- beam of 40 GeV/c on a polarized target [14] (Fig.9).
- π^0 mesons using an antiproton beam of 40 GeV/c on a polarized target [15] (Fig.10).

Large asymmetries are observed in several of the above reactions. The magnitude of the effect is strongly dependent on the type of the produced particle (note a small asymmetry for observed π^- and large asymmetries for observed π^+ and π^0). Their origin is as yet unclear. Since all the above experiments have been limited to incident beam momenta lower than 40 GeV/c and to transverse momenta of the observed particle smaller than 3 GeV/c, it is uncertain whether one is in the domain of hard scattering where perturbative QCD can be applied. Naive perturbative QCD estimates single transverse spin asymmetries for the production of a particle of transverse momentum p_T to vanish as $\alpha_S m_q/p_T$ where m_q the quark mass and α_S the strong coupling constant [17]. More detailed analysis shows that a simple factorization form, as assumed in the naive estimate, does not hold [18]. The relevant mass parameter may be the hadron mass [19]: then the calculation of the imaginary part matters. It still leads to small asymmetries different for qq [19] and $\bar{q}q$ sub-processes [20]. Two approaches [21, 22], involving unmeasured structure functions, show that higher twist effects have to be invoked: either parton correlation densities [21] or structure functions dependent on the transverse momentum of the constituents [22]. Experimental measurements at high transverse momentum would help to understand the subtleties inherent to transverse spin.

The asymmetry in prompt photons production has never been measured. This process is interesting since only two subprocesses, at leading order, are relevant : The "QCD Compton" $gq \rightarrow \gamma q$ and the annihilation $\bar{q}q \rightarrow \gamma g$. The Compton diagram dominates in pp interactions while the annihilation diagram is important in $\bar{p}p$ interactions at high x_T. Full next-to-leading order calculations [23] of the cross-sections allow a detailed comparison with experiments [24]. The SPS direct photon data obtained with incident pions, protons and antiprotons constrain the QCD scale parameter $\Lambda_{\overline{MS}}$ to a value [25] consistent with that

obtained from an analysis of scaling violations in DIS [26]. The applicability of QCD to this channel at SPS energies is thus firmly established by the cross-section analysis. The measurement of single spin asymmetries in direct photon production at high p_T and very high x_T using both proton and antiprotons as incident particles must surely help to understand transverse spin.

It is the intention of UA6 to extend these measurements to the production of π^0, η, ω^0 and direct photons up to p_T of 6 GeV/c using both protons and antiprotons of 315 GeV/c incident momentum. The asymmetry in J/ψ production will also be measured.

2.2 Asymmetry in Λ production

Λ hyperons produced in high energy pp collisions have been observed to have large polarization perpendicular to their production plane, as allowed by parity conservation. This surprising effect has not met a satisfactory explanation for more than a decade. The polarization data lie in a rather low transverse momentum region where perturbative QCD calculations are not expected to be applicable. Several ad-hoc models attempted to explain with more or less success the polarization of the Λ : in the semi-classical approach of the Lund group [27], the polarization of the valence quark s arises from local conservation of angular momentum, the $s\bar{s}$ pair being created with angular momentum l in the confining color field. DeGrand and Miettinen have proposed a model in which the Λ polarization arises from the Thomas precession of the s quark. Their model also predicts spin correlation between the initial baryon and the produced hyperon [28].

With a polarized target, further tests of these models can be performed by the measurement of two additional spin parameters, the asymmetry (or analyzing power) A_n and the transverse spin transfer D_{nn}. For direct Λ production, the initial spin state is predicted to have no effect on the production rate nor on the final hyperon polarization. In our experiment, however, we do not distinguish between direct Λ and Λ from Σ^o decay, as the accompanying γ might not be detected; the predictions of the models have to be modified to account for those Λ, as Σ^o might keep some memory of the spin in the initial state.

The present set-up does not provide the means to trigger on Λ. The original Λ triggering scheme was to trigger on a multiplicity increase between the first and the second chamber before the magnet. The large multiplicity in the front chambers has made this scheme inoperative. A new triggering scheme is now

under study and involves correlation searches between scintillator pads located behind the magnet and after the last MWPC as a first level trigger, the second level being based on a transputer network which allows parallel analysis on the data of the MWPCs.

It is the intention of UA6 to measure transverse single spin asymmetries and spin transfer parameter D_{nn} in the kinematical region $-0.1<x_F<0.3$.

3. THE POLARIZED ATOMIC BEAM TARGET

The target (fig. 11) consists of a well defined high density atomic hydrogen beam with a high degree of polarization. Among the methods being at present considered for this application, we have chosen an optimized version of the 'classical' atomic beam with a single passage through the accelerator beam. This approach has several important advantages:

- the size of the interaction region is 3 mm transverse and 30 mm along the beam. It can be considered as point-like for transverse measurements.
- no material in the immediate vicinity of the target.
- operation with deuterium will be possible.

To a large extent the polarized beam target is similar to the atomic beam part of polarized ion sources. The best density values published for such a beam are 2.10^{12} atoms/cm^3 inside a diameter of about 1 cm, adapted to the size of an electron beam ionizer at ETH Zürich [29]. Since we will only select one hyperfine state (the ion source at ETH Zurich selects two), a direct copy would give 1.10^{12} atoms/cm^2. We aim at a target thickness of 1.10^{13} atoms/cm^2 and intend to achieve this improvement in essentially two ways:

- increase the **acceptance** by using superconducting sextupoles with higher poletip fields (4 T compared to about 1 T in the ETH design) and larger aperture (30 to 100 mm compared to 20 to 30 mm at the ETH).
- increase the **gas input** by using a larger aperture rectangular nozzle.

From theoretical considerations, it follows that we can expect a target thickness of up to 1.10^{13} atoms/cm^2 with a minimum of 4.10^{12} atoms/cm^2 [30]. We will use this latter conservative figure in the subsequent event rate calculations. The expected cross section of the atomic beam at the SPS beam will be 30x5 mm^2.

The main uncertainty in the above thickness calculation is in the maximum possible gas input, since there exists no good theory to describe properly the expansion region near the nozzle.

The first three stages of the vacuum system will be pumped by turbomolecular pumps, while the rest of the beam production system will be pumped by cryo-surfaces. It is estimated that a regeneration of these surfaces will be necessary once a week.

Particular care will be taken to keep the background gas pressure in the target region as low as possible by improving the dump design compared to the existing molecular beam target. The valve between SPS-vacuum and the dump will have a diameter of 150 mm (35 mm in the present jet), and the cryopump will be raised through this valve up to the aperture limit of the accelerator. Besides absorbing the well collimated target beam, the pump will have an effective pumping speed of about 10000 l/s for diffuse hydrogen, and we expect a background pressure of less than 10^{-7} mbar in spite of the larger diaphragms compared to the cluster jet (see table 1 for a comparison with the existing molecular jet target).

A set of coils around the target region will produce a small orienting magnetic field (60 to 100 Gauss) to align the spin in any direction required by the experiment. The direction of the field, and hence of the spin orientation, can be switched frequently, say every second, to reduce systematic errors.

The design of the superconducting sextupoles has been started in collaboration with magnet experts and it seems that the required performance is technically feasible.

3. 1 Luminosity

The instantaneous luminosity is given by:

L= (target thickness) x (beam intensity) x (revolution frequency)

In order to calculate the luminosity we shall assume the following:

- a polarized target thickness of $4 \cdot 10^{12}$ atoms/cm^2. This is a conservative factor of 100 lower than the present molecular jet.

- 10^{12} protons and $5 .10^{11}$ antiprotons circulating in the SPS at a revolution frequency of 43.4 kHz.

With these values we obtain :

an instantaneous $\bar{p}p$ luminosity $L_{\bar{p}p} = 8.7 .10^{28}\ cm^{-2}. s^{-1}$

an instantaneous pp luminosity $L_{pp} = 1.75 .10^{29}\ cm^{-2}. s^{-1}.$

3. 2 Comparison with the existing molecular hydrogen jet target

The basic parameters of the polarized atomic beam target, compared to our existing molecular hydrogen jet target, are listed below.

Table 1 **Comparison of the atomic beam target with the molecular jet target.**

	Polarized atomic beam target	Molecular jet target
Target thickness atoms/cm^2	4.10^{12} to $1 .10^{13}$	$3 .10^{14}$
Target dimension along the beam cm	3	0.8
Background gas pressure mbar	$< 10^{-7}$	$< 10^{-6}$
Polarization	> 0.9	
Magnetic field in target region T	0.005 - 0.010	
Luminosity ($\bar{p}p$) cm^{-2} s^{-1}	(0.9-2.25) x 10^{29}	7.0 x 10^{30}
Figures of merit pp	$F_p \geq 1.7 .10^{29}$	
Figures of merit $\bar{p}p$	$F_{\bar{p}} \geq 7.2 .10^{28}$	

The integrated luminosity for a 100 day $\bar{p}p$ run at 50% running efficiency can be computed as:

$(8.7\ 10^{28}\ cm^{-2}.s^{-1})$ x $(100 \times 8.6410^{4}\ s)$ x $(0.5) = \mathbf{3.8 \times 10^{35}\ cm^{-2} = 380\ nb^{-1}}$.

The expected pp luminosity is twice as high.

3. 3 Polarization

The effective target polarization can be defined as

$$P = (T^{+} - T^{-}) / T$$

with T^{+} (T^{-}) the target thickness with wanted (unwanted) spin states, and T the total target thickness. The target thickness as seen by the accelerator beam is made up of

- atoms in state 1, fully polarized by the low orienting field (< 0.01T) at the target point
- some atoms in state 2, left here because of the inefficency of the RF-transition. This state remains unpolarized in the low orienting field at the target point
- some atoms in states 2 and 4, left here due to incomplete elimination by the sextupoles. These states also remain unpolarized in the low orienting field at the target point
- atoms depolarized by the passage through the accelerator beam
- residual unpolarised gas molecules

R, the counting rate ratio, is defined as the ratio of counting rates with RF-transition off and on. In table 2 the contributions to target thickness T, the polarization and counting rate ratio R are compared for a fully efficient and 95% efficient RF-transition , neglecting the depolarisation due to the beam crossing.

Table 2 Contributions to target thickness T , polarization and counting rate ratio R.

	T atoms/cm^2 RF eff. 100%	T atoms/cm^2 RF eff. 95%
state 1	9.73 .10^{12}	9.73 .10^{12}
state 2	1.1 .10^{11}	5.9 .10^{11}
state 3	--	--
state 4	0.8 .10^{11}	0.76 .10^{11}
background (10^{-7}mbar)	0.5 .10^{11}	0.5 .10^{11}
total	9.97 .10^{12}	1.04 .10^{13}
polarization	0.976	0.93
Counting ratio R	1.95	1.86

Since an atom never meets more than one bunch (atom speed 1 mm/μs , bunch spacing 3.8 μs), depolarization is unlikely. Residual gas pressure will be low, so that the polarization will be determined mainly by the quality of the RF-transition (see table 2).

In order to measure and monitor the polarization, we have considered three methods:

- elastic scattering in the Coulomb interference region
- atomic beam polarimeter (a combination of RF-transitions, sextupole and mass spectrometer after the beam dump, see fig.11)
- counting rate with RF-transition on/off.

The first method relies on the detection of the low energy recoil of pp ($\bar{p}p$) elastic scattering at small momentum transfer ($0.002<t<0.03$ (GeV/c)^2) with a recoil spectrometer based on position sensitive silicon detectors. Previous measurements have shown that by detecting the recoil only, elastic scattering can be selected with a background smaller than 10%. The polarization parameter

P for this reaction, essentially produced at very small momentum transfer by the interference of the non-flip amplitude (Pomeron exchange) and an electromagnetic spin flip amplitude (charge - magnetic moment interaction) , can be calculated in the hypothesis of vanishing hadronic spin flip:

$$P(t) = \frac{\frac{\alpha(\mu-1)}{2m}\,\sigma_T\,|t|^{-\frac{1}{2}}}{\frac{\sigma_T^2}{16\pi} + 4\alpha^2\pi\,|t|^{-2}}$$

This expression reaches a sharp maximum at $|t| = 3.10^{-3}$ $(GeV/c)^2$ and a measurement of the corresponding asymmetry is a direct verification of the absence of spin flip in Pomeron exchange and can also be used as a calibration measurement for the target polarization. As the cross section for this reaction is rather large ($d\sigma/dt$ = 100 mb $(GeV/c)^{-1}$) this measurement can be performed with high precision rather quickly and could be repeated occasionally to check the target stability.

For a measurement of the asymmetry of the |t| - distribution with 1% accuracy one week of data taking would be necessary; a monitoring measurement of the average asymmetry would give a 5% measurement of the target polarization in 2.5 hours at a luminosity of 4.10^{29} $cm^{-2}s^{-1}$.

This method allows to measure the target polarization at the beam (except for the contribution of the residual gas, for which the acceptance is too different from the acceptance of the forward detectors). But due to the geometry of the target it requires a vertical polarization, incompatible with the horizontal one prefered for inclusive reactions and will be measured separately.

The atomic beam polarimeter located after the beam crossing consists of two RF-transitions, one transition $1 \rightleftharpoons 3$ and one transition $2 \rightleftharpoons 4$, followed by a short permanent sextupole and a mass spectrometer (see fig.11). To give an idea of the sensitivity of the method, table 3 shows the spectrometer current for various combinations of RF-transitions on/off . Cases A and B correspond to column 1 and and 2 of table 2, case C to column 2 of table 2 but with 5% of level 1 atoms having made a transition to level 3 in passing through the SPS vacuum chamber. It can be seen, that changes in RF-Transition efficiency and depolarization can clearly be detected.

Table 3 **Signal measured by the atomic beam polarimeter normalized to a situation where all R-F transitions are switched off.**

RF-Transitions			Cases		
1 (2⇌4)	2 (2⇌4)	3 (1⇌3)	A	B	C
Off	Off	Off	1	1	1
On	Off	Off	0.52	0.55	0.55
Off	On	Off	0.50	0.50	0.50
Off	On	On	0.017	0.017	0.042

The method has the advantage of simplicity, but only measures the states distribution in the beam sample accepted by the polarimeter, not the actual target polarization. Nevertheless it will allow a continuous monitoring of the operating conditions with a precision of about 5%, independent of the polarization direction in the interaction region.

Switching the RF-transition off should (almost) double the target density. It is a fast check of atomic beam production, in particular RF-transition efficiency, also independent of direction of target polarization. A further cross-check would be the measurement of polarization under this condition (should be about 50%).
We intend to pursue the following strategy :

- Twice per run (at the beginning and at the end) the target polarization is determined with precision with the elastic scattering method (about a week each). Although the polarization direction required is not optimal for the rest of the experiment, the time can be used for detector studies, trigger set up etc.

- At regular intervals, the counting rate ratio is determined by switching off the RF-transition (say, one minute per hour).

- The atomic beam polarimeter is working all the time and acts as a permanent monitor of the target beam polarization, independent of the polarization direction at the target point.

3.3 Comparison with existing facilities

Solid polarized targets

The advantages of a polarized jet over existing polarized targets are many:

- A high degree of polarization (90%). Thus any "physics" asymmetry is not diluted by interactions occuring in bound unpolarized nucleons. For example in [13] a propanediol ($C_3H_8O_2$) target was used and the physics asymmetry was reduced by a dilution factor of about 10. Conversely when going from a raw to a final asymmetry systematic errors are multiplied by the same factor of 10. Moreover this dilution factor varies with rapidity and transverse momentum.
- The spin of the protons in the jet is aligned using a weak orienting magnetic field over the interaction region. It can therefore be reversed by merely changing the direction of current flow in a coil. The frequency of polarization reversal can therefore be several Hz. In contrast in a propanediol target the polarization is reversed every two hours. This frequent reversal will reduce systematic errors.
- The low density of the jet allows very low energy recoil protons (about 1 MeV) to be observed in solid state detectors placed inside the vacuum [5]. This allows the monitoring of polarization using elastic scattering in the Coulomb-nuclear interference region .
- The small longitudinal dimension of the target allows easy computation of transverse momenta in real-time, straightforward clustering algorithms and discrimination against particles not originating at the interaction vertex.
- Radiation damage which is a problem for most solid polarized targets is of course irrelevant for the jet target.

Polarized beams

The only existing high energy polarized beam is the 200 GeV proton and anti-proton beam at the Fermilab Tevatron (the Brookhaven polarized beam is limited to about 20 GeV). This new facility will be taking physics data in 1990 and is characterized by the following main features:

- a beam of 200 GeV/c protons or antiprotons,

- an intensity of 3.10^7 protons/spill or $1 .10^6$ antiprotons/spill, where a spill occurs once every 60 seconds,
- a tagged polarization of 40 %. The position of the incident particle must be known accurately as the polarization reverses across the profile of the beam. The polarization distribution at the target is reversed every 10 minutes using a Siberian Snake.
- an achievable luminosity with a 1m long liquid hydrogen target of :

$$L_p = (3 .10^7 / 60) \times (4 .10^{24}) \text{ cm}^{-2}\text{s}^{-1} = 2 .10^{30} \text{ cm}^{-2}\text{s}^{-1}. \text{ for protons}$$

$$L_{\bar{p}} = (1 .10^6 / 60) \times (4 .10^{24}) \text{ cm}^{-2}\text{s}^{-1} = 7 .10^{28} \text{ cm}^{-2}\text{s}^{-1}. \text{for antiprotons}$$

- the respective figures of merit are

$$F_p = P^2L = 3 .10^{29} \text{ cm}^{-2}\text{s}^{-1} \text{ for protons}$$

$$F_{\bar{p}} = 1 .10^{28} \text{ cm}^{-2}\text{s}^{-1} \text{ for antiprotons.}$$

Even with the lowest target thickness envisaged (4.10^{12} at/cm^2, see table 1) it appears that the UA6 polarized jet figures of merit will be comparable for protons and appreciably better for antiprotons. It is to be noted however that UA6 will run at higher energy (315 instead of 200 GeV) which is very important at high p_T, and will be better as far as beam purity, degree of polarization and target size are concerned.

4. RATES

4.1 Asymmetry in π^0 and η production

Our first publication on π^0 and η production was based on 43 nb^{-1}. Assuming an unmodified detector and given the 380 nb^{-1} derived above, we can expect approximately 9 times more events than in our publication (see Table I). The published π^0 cross-section extends to p_T = 5 GeV/c (fig. 1). One can therefore expect to measure asymmetries in π^0 and η production up to about 6 GeV/c. The expected statistical errors based on the calculated numbers of events are listed in columns 4 and 6 of Table 4 for π^0 and η respectively.

Table 4 π^0 and η Asymmetry

P_T range	π^0's in Ref. [3]	Expected π^0	Error on π^0 asym.	Expected η	Error on η asym.
2.7-2.9	923	34668	0.006	4376	0.03
2.9-3.3	3136	27713	0.007	3980	0.03
3.3-3.7	839	7414	0.013	1260	0.05
3.7-4.1	203	1794	0.026	296	0.10
4.1-5.1	78	689	0.042	128	0.15

As mentioned earlier, an experiment at Brookhaven has observed a large asymmetry in π^+ production and essentially no asymmetry in π^- production. The experiment was limited to $p_T < 2$ GeV/c with an incident beam of 28 GeV.

4.2 Asymmetry in J/ψ production

We have extracted a J/ψ signal from our 1985 and 1986 data samples [6]. With 540 nb^{-1} and a 58% trigger efficiency 102 events were observed in $\bar{p}p$. The low trigger efficiency was due to an inefficient gain control on the trigger scintillators. With a more efficient trigger and the expected integrated luminosities computed above a sample of 125 J/ψ in $\bar{p}p$ and 170 in pp should be collected. Our J/ψ data are consistent with models that predict that in pp collisions J/ψ are produced primarily via gluon fusion whereas in $\bar{p}p$ collisions both gluon fusion and $q\bar{q}$ annihilation are responsible. Therefore an observation of different transverse asymmetries in pp and $\bar{p}p$ collisions could give a clue as to the origin of single spin asymmetries.

4.3 Asymmetry in direct photon production

The expected number of events in a 100 day run, based on the numbers of events in our publication [4], is given in Table 5 as a function of p_T , together with the error in the asymmetry including the background subtraction. An error of 10% on the asymmetry can be achieved up to a transverse momentum of 5 GeV/c.

Table 5 Direct Photon Asymmetry

P_T range	Expected γ	Error on Asymmetry
3.3-3.5	795	0.06
3.5-3.7	598	0.07
3.7-3.9	354	0.09
3.9-4.1	220	0.10
4.1-5.1	300	0.09

4.4 Asymmetry in Λ production

The rate of production of the Λ has been estimated using the parametrization of Pondrom [31] extrapolated to our kinematical domain. For a period of 100 days running at 70% efficiency, we estimate that the total number of Λ detected in our apparatus would be $1.75 \cdot 10^6$ for each orientation of the target polarization. This would allow to reach transverse momenta around 2 GeV/c : at this value of p_T, the relative error on the asymmetry will be 35% for an asymmetry of 5%.

4.5 Possible increase in luminosity

We have considered ways of increasing the luminosity. For $\bar{p}p$ running, this will be impossible because of the limitation of the $\bar{p}$ source. For pp running we have considered three ways of increasing the beam intensity. An increase of the number of protons per bunch could at most produce a gain by a factor of two. Increasing the number of bunches could also be considered. Another factor of two may be obtained but would require substantial machine development studies. The most effective way, which will give the highest luminosity, is by coasting a debunched beam. The usual 3.10^{13} protons accelerated in the fixed target mode of operation of the SPS could be stored. This would provide an instantaneous luminosity of 6.10^{30}. Therefore, running in a dedicated mode of operation of the SPS during a full month of data taking we could reduce the error on the asymmetry parameter in direct photon production from approximately .080 per p_T bin (see table 5) to .025.

5 THE APPARATUS

5.1 Present set-up

The set-up of experiment UA6, shown in Fig. 12, is located in a 12m long straight section of the SPS. It consists of a hydrogen cluster jet used as an internal target followed by a double-arm spectrometer. The angular coverage of each arm is 20 to 100 mrad in polar angle and 70^{o} in azimuth, corresponding to 1.8 sr in the centre-of-mass. Photons and π-mesons are detected in the rapidity (y) range of -0.40 to +1.25. An arm consists of: five multiwire proportional chambers (PC), one in front and four behind a 2.3 T.m magnet; a Li/Xe transition radiation detector; and an electromagnetic (e.m.) calorimeter.

The two e.m. calorimeters [32] are of the lead-proportional tube type. Each calorimeter consists of 30 lead plates, each plate 0.8 radiation length (X_0) thick, interleaved with alternating layers of horizontal and vertical tubes of 1 cm transverse dimension and 0.5 cm depth. The tubes are filled with a mixture of Argon-CO_2 and are operated at a gas amplification of about 1000. Each calorimeter is divided longitudinally into three modules of $8X_0$ each. In order to reduce the number of read-out channels, the analog signals of the tubes directly behind one another are summed within a module. This preserves the fine lateral segmentation of the calorimeter, which is essential for good γ/π^{o} discrimination and provides three longitudinal samplings for good e.m. shower identification. The position resolution for showers was found to be 3.5 mm (r.m.s.) at 10 GeV, improving to 1.5 mm at 75 GeV. The minimum resolved two-shower separation is 2.8 cm. Test-beam results show that the calorimeter response to electrons in the range 10 to 100 GeV is linear to better than 0.6% and that the energy resolution is given by $\sigma(E)/E=0.29/\sqrt{E}$ (E in GeV). The overall energy scale of the calorimeter is determined and adjusted on an hourly basis, by centering the π^{o} mass peak at its known value.

In 1987, as part of the upgrade, another module referred to as CALUP, was added to each calorimeter between the first and second modules. CALUP consists of three planes of proportional tubes of 0.5 cm transverse dimension and 1 cm depth. One plane is made up of horizontal tubes and the other two of tubes inclined at $\pm 60^{o}$ to the vertical. The purpose of CALUP was

- to provide a means of removing ambiguities when matching horizontal tube clusters with vertical tube clusters in multi-photon events.
- to improve the two-shower separation using its finer granularity (5 mm tubes instead of 10 mm in the original calorimeter).

A hodoscope consisting of seven horizontal scintillation counters, the T_0 counters, was located between the first and second calorimeter module. The pulse height in these counters is proportional to the e.m. energy incident on the calorimeter. They were used as a pretrigger with a rate of a few kilohertz. These events were then examined by a hardware processor which

- read the analog sum of groups of 6 adjacent calorimeter channels of the first and second modules into fast ADC's;
- grouped the energy in the calorimeters into overlapping bands of 12 channels in both vertical and horizontal views;
- summed each horizontal band with each vertical band. Then, assuming that the energy was deposited at the geometrical intersection of the two bands
- it converted it into a p_T and accepted the event if this p_T exceeded the minimum required , typically 3 GeV/c;
- and, in the case of energy deposited in both calorimeters, it computed the invariant mass and accepted the event if this mass was above a minimum mass, typically 2.5 GeV/c^2.

During the 1987 upgrade the vacuum chamber in front of the magnet was considerably lightened in order to minimize secondary interactions in it. Instead of stainless steel it was made of aluminium. Its shape was also changed from an ellipse 43 mm high to a cylinder 70 mm in diameter.

5.2 Proposed additions and modifications

Λ Fast Processor.

As already mentioned the present set-up does not provide the means to trigger on Λ . It is now intended to use a two-level trigger that would retain events with two tracks intersecting downstream of the jet or one high p_T track. This scheme would consist of:

- A Track First Level Trigger (**TFLT**) defined by two planes of scintillator pads placed down-stream of the spectrometer magnet. At a luminosity of $2 .10^{29}$ $cm^{-2}s^{-1}$ the interaction rate is 7000 s^{-1}. The TFLT , using NIM logic, would reduce this by about a factor of 20 between bunch crossings (3.8 μs) and would introduce no dead-time.
- A Track Second Level Trigger (**TSLT**) based on a Transputer Network. This network will be interfaced to our MWPC electronics, the Receiver Memory Hybrid (**RMH**) system, to perform parallel acquisition and data analysis on the 350 events/sec surviving the TFLT.

A Transputer is a 32 bit processor built by INMOS (UK) which includes on the same chip:

-an internal fast memory (2.4 kbytes),
-four bidirectional high speed serial links,
-an optional Floating Point Unit (**FPU**).

The information from each of our MWPC planes (coded in one bit per wire) will be read through the RMH crate encoders by a transputer-based module, the Parallel Acquisition Crate (**PAC**). The whole MWPC information can be read in 10μsec. The PAC will then make this information available for parallel processing (space point calculation, track fitting, momentum calculation, secondary vertex computation) by further modules also using Transputers. We estimate that the calculation of the vertex position of two tracks intersecting downstream of the jet will take 300μsec. Requiring this vertex to be distinct from the jet position (note that the jet is only 30mm long) will allow the TFLT rate to be reduced by a factor of 50. Thus the event rate to tape should be about 7 Hz for this trigger. It is to be noted that:

- two PAC modules **have already been built** and are currently being tested,
- a preliminary version of another necessary module, the New System Encoder (**NSE**) which will handle pretrigger information, activate parallel reading, control the analysis stage and manage the serial transfer of data between the PAC's and the online computer for the accepted events **has also been built** and is being evaluated.

New Calorimeter Trigger Processor and T_0 Scintillators

As described earlier the present processor sums strips of 12 horizontal and 12 vertical tubes and assumes that the resulting energy was deposited by a single particle incident in a $12x12cm^2$ square. However, many triggers are in fact due to several particles each of which is below the required p_T threshold, incident on the same strip. This results in many unwanted triggers and a consequent increase in the minimum p_T threshold that we can require in order not to introduce too much dead-time. These spurious triggers would be eliminated if we could trigger on the energy actually deposited in a square. This is clearly not possible using the calorimeter because of the tube construction. On the other hand replacing the existing T_0 by a mosaic of scintillator tiles would allow us to form clusters of adjacent tiles and trigger on their energy content. Since the scintillator is located between the first two modules of the calorimeter the energy deposited in it by an electromagnetic particle is proportional to its energy. Fig. 15 shows a possible layout of the new T_0 scintillator tiles for the top arm of the calorimeter. The tiles would be read by wavelength-shifting fibers embbeded in the tile sufaces which carry light to phototubes located next to the calorimeter. Prototypes have already been built and have been evaluated in a test beam.

An existing splitter-mixer system would serve as a new calorimeter trigger processor. It allows us to form analog sums of ovelapping groups of scintillator tiles. p_T thresholds are applied to the sums using computer-controlled discriminators between bunch crossings resulting in no dead-time. A new two-arm mass-trigger would also be used. It would use the scintillator tiles pulse height as input into a FERA (Fast Encoding and Readout ADC) system which also already exists.

6 BUDGET

The budget can be divided essentially into two parts: the polarized atomic beam and improvements to the detectors. Some components for the polarized atomic beam already exist, further spending is estimated to be 800 KSF. The global budget to build the polarized atomic beam and to modify the detectors as described above is summarized in table 6.

	Cost KSF
Polarized atomic beam	800
Λ pretrigger	200
Λ processor	300
To counters	100
Vacuum pipe and magnet modifications	50
Repair of calorimeter	50
total	1600
contingency (15%)	200
Estimated cost	1800

Table 6 Budget

7 TIME SCALE

Starting to work on the final design of the atomic polarized beam at the beginning of 1990 we can expect to have the target ready in the second half of 1991.

The T0 scintillators and the Λ processor could be ready and tested during the 1990 collider run. The rest of the processor will be ready by the end of 1991.

A minimum of two running periods will be needed, one for measurements in $\bar{p}p$ mode and one for measurements in pp mode. These two periods should be separated by at least a 6 to 8 week shut down to allow us to switch from one mode to the other by rotating the whole apparatus. These periods could be scheduled during normal collider operation, or during short dedicated periods of single debunched coasting beam, if collider running is discontinued (see section 4.5).

8 CONCLUSION

The introduction of a polarized jet in the UA6 set-up, in 1991, would allow us to study single-spin asymmetries in π^0, η, ω^0 , Λ and direct photon production in both pp and $\bar{p}p$ interactions up to p_T of 6 GeV/c at a $\sqrt{s}$ of 24.3 GeV. This is clearly in a domain where hard scattering ideas can be applied. In particular the results could be conpared with perturbative QCD predictions. In this comparison with theory it will clearly be an advantage to have results on several particles and with two initial states. In addition the asymmetry in J/ψ inclusive production could also be measured.

A strong case can be made why CERN should continue the development of the polarized atomic beam target. The existing molecular cluster jet has operated successfully and reliably for several years. An experienced development team exists at CERN. This team has recently been strengthened by an Italian group. Furthermore an existing experiment would put the target to immediate use. The applicability to LEP in the near future is a distinct possibility.

It should also be noted that many members of our group have done polarization experiments, and indeed, participated in the various pioneering experiments at high energies at the CERN PS, the CERN SPS, the Fermilab Hyperon Beam, the Fermilab Polarized Beam, at Brookhaven and at SLAC. We are also in contact with groups at Frascati and in the USSR who are interested in the physics goals of the experiment and could decide to join us.

Appendix 1

Basic design of the Polarized Atomic Hydrogen Beam Target.

The polarized atomic hydrogen beam target is based on the separation of atoms in different ground state hyperfine levels in inhomogenous magnetic fields. As shown in fig.13 (Breit-Rabi diagram) , the ground state of the hydrogen atom in a magnetic field splits into four hyperfine levels. The force on an atom in an inhomogenous magnetic field [34]is given by

$$F = - \text{grad } W = -\partial W / \partial B \text{ grad } B = - \mu_{eff} \text{grad } B$$

With W the potential energy of the atom. The effective magnetic moment $\mu_{eff} = \delta W/\delta B$ being different for different hyperfine levels, they may be separated in an inhomogenous field. In particular, in a sextupole field atoms in level 1 and 2 perform a sinusoidal motion, while the trajectories of atoms in levels 3 and 4 are of hyperbolic sine shape.

The general layout of the target has already been shown in fig.11. A schematic diagram is given in fig.14. At first, hydrogen is dissociated in a low pressure radiofrequency discharge and through a nozzle the atoms pass into a vacuum sufficiently low to avoid any collisions. A first sextupole eliminates most atoms in levels 3 and 4, atoms in levels 1 and 2 stay in the beam. Such a mixture of levels has no nuclear polarization at high magnetic field, and only 50% nuclear polarization at low fields. A suitable combination of a RF-field and a dipole magnetic field ("RF-transition") induces an exchange of population of levels 2 and 4. The result is a beam of atoms in levels 1 and 4 . The second sextupole again eliminates atoms in level 4, and the beam now essentially consists of atoms in level 1, with full nuclear polarization at any field level. The direction of polarization is given by a dipole field of about 60 Gauss created by one out of three pairs of coils around the interaction region. After passage through the accelerator the beam is absorbed by a cryopump.

The density of the target beam is determined by limitations at several stages of the system:

- The dissociator: From experience it is known that the best output of hydrogen atoms is achieved with pressures around one millibar. At higher

pressures, the dissociation degree decreases rapidly due to volume recombination.

- The nozzle-skimmer region: The flow processes in this region are not yet well understood [33]. The flow inside the nozzle is friction-limited ("slip flow"), and the expansion into the vacuum results in a velocity distribution with mean velocity and width depending on nozzle temperature. The forward intensity seems to be proportional to nozzle aperture . As explained in the following paragraph the acceptance of the optical system increases with decreasing beam velocity, therefore the nozzle is cooled to a temperature around 30K. At even lower temperatures the forward intensity rapidly decreases due to recombination on the nozzle surface.

- Optical system: It can be shown that the acceptance of a multipolar field is proportional to B_p/v^2, with B_p the field at the pole-tip and v the atom velocity. In addition to cooling the atoms as described above we can increase the acceptance by increasing the pole-tip field. Classical magnets have fields up to 1T, with optimized permanent magnets a value of up to 1.5 T may be achievable. We plan to use superconducting sextupoles with pole-tip fields up to 4 T, which is possible with existing wire technology. By a careful choice of geometry (magnet aperture and length, distance between the magnets) the transmission between nozzle and target point can be optimized.

- Atomic beam scattering: The fraction of atoms actually arriving at the target point is only about 1.5% of the total gas input, the rest has to be pumped away by a very efficient differential pumping system. Particular attention has been given to the region of the first sextupole, where the mean free path may become of the order of the magnet length.

REFERENCES

[1] Study of Spin Effects in pp Reactions at SPS using a Polarized Atomic Hydrogen Jet Target, CERN/SPSC/77-7, SPSC/P 88.

[2] Proposal for the Study of e^+e^-, γ, π^0 and Hyperon Production in pp Reactions at $\sqrt{s}$ = 22.5 GeV using an Internal Jet Target at the SPS.CERN/SPSC/80-63, SPSC/P 148.

[3] J. Antille et al, Phys.Lett.**194B** (1987) 568.

[4] A. Bernasconi et al, Phys. Lett. **206B** (1988) 163

[5] R.Breedon et al, Phys. Lett. **216B** (1989) 459

[6] A. Bernasconi et al, submitted to the Int. Europhysics Conf. on High Energy Physics, Madrid, 1989

[7] Addendum to Proposal: Proposal for the Study of e^+e^-,γ,π^0 and Hyperon Production in pp Reactions at $\sqrt{s}$ = 22.5 GeV using an Internal Jet Target at the SPS. CERN/SPSC/86-35, SPSC/P 148/Add. 1

[8] J.Antille et al, Nucl. Phys. **B185** (1981) 1,
P.R.Cameron et al, Phys. Rev. **D32** (1985) 3070,
J.H.Snyder et al, Phys. Rev. Lett. **41** (1978) 781,
G.Fidecaro et al, Phys. Lett. **105B** (1981) 309.

[9] For a review of hyperon polarization see K.Heller p. 81, Vol. 1, Proc. of the VII International Symposium on High Energy Spin Physics , Protvino, September 1986.

[10] S.Erhan et al., Phys. Lett. **B82** (1979) 301.

[11] W.H. Dragoset et al., Phys. Rev. **D18** (1978) 3939.

[12] Y.I. Makdisi, p. 53, Vol. 1, Proc. of the VII International Symposium on High Energy Spin Physics , Protvino, September 1986.
S. Saroff et al., AZPH-Ex/89-01 Submitted to Phys.Rev.Lett.

[13] J. Antille et al, Phys. Lett. **94B** (1980) 523.

[14] V.D.Apokin et al., p.83, Vol. 2, Proc. of the VII International Symposium on High Energy Spin Physics , Protvino, September 1986, submitted to Yad. Fiz (IFVE 89-37)

[15] V.D.Apokin et al., p.86, Vol. 2, Proc. of the VII International Symposiumon High Energy Spin Physics , Protvino, September 1986.

[16] J. Ashman et al. Phys. Lett. **206B** (1988) 364.

[17] G. Kane, J. Pumplin and W. Repko, Phys. Rev. Lett. **41** (1978) 1689.

[18] N. S. Craigie, K. Hidaka, M. Jacob and F. M. Renard,
Phys. Reports 99 (1983) 69,
N. S. Craigie, Proc. of the Int. Symp. on High-Energy Spin Physics,
Upton 1982, p292.

[19] A. V. Efremov and O. V. Teryaev, Sov. J. Nucl. Phys. **36** (1982) 140.

[20] G. M. Zinov'ev and A. M. Singriev, Sov. J. Nucl. Phys. **45** (1987) 908.

[21] A. V. Efremov and O. V. Teryaev, Phys. Lett. **150B** (1985) 383,
A. V. Efremov, Proc. of the VII Int. Symp.on High Energy Spin Physics,
Vol. 1, p89 Protvino, sept. 1986,
P. G. Ratcliffe, Proc. 6th Int. Symp. on High Energy Spin Physics,
Marseille 1984, Journal de Physique, C2, tome 46 (1985) C2-31,
P. G. Ratcliffe, Nucl. Phys. **B264** (1986) 492.

[22] D. Sivers, ANL-HEP-PR-89-32.

[23] P.Aurenche, R. Baier, A. Douiri, M. Fontannaz, D. Schiff, Phys. Lett. **B140** (1984) 87.

[24] P.Aurenche, R. Baier,M. Fontannaz, D. Schiff, Nucl. Phys. **B297** (1988) 661.

[25] P. Aurenche,R. Baier,M. Fontannaz,J. F.Owens,M. Werlen, Phys Rev **D39** (1989) 3275,
P. Aurenche, R. Baier, M. Fontannaz, M. N. Kienzle-Focacci, M.Werlen, to appear in Phys. Lett. B.

[26] A. C. Benvenuti et al., Phys. Lett. **223B** (1989) 490.

[27] B. Anderson, G. Gustafson and G. Ingelman, Phys.. Lett. **B85** (1979) 417

[28] T. A. DeGrand and H. I. Miettinen, Phys. Rev. **D23** (1981) 1227
T. A. DeGrand and H. I. Miettinen, Phys. Rev. **D24** (1981) 2419
T. A. DeGrand, J. Markkanen and H. I. Miettinen, Phys. Rev. **D32** (1985) 2445

[29] W. Gruebler et al., Proc. Int. Workshop on Pol. Sources and Targets, Montana, 1986 (HPA **59** 1986)

[30] L. Dick, W Kubischta, CERN-EP/88-135, to be published in Proc. 8th Int. Symp. on High Energy Spin Physics, vol II p 1518, Minneapolis 1988.

[31] L.G. Pondrom, Phys. Reports **122** (1985) 58

[32] L. Camilleri et al., to appear in NIM

[33] A. Hershkovitch, A. Kponou and T. O. Niinikoski, Rev. Sc. Instr. 58 (1987) 547

[34] W. Haeberli, Ann. Rev. Nuclear Science **17** (1967) 373

FIGURE CAPTIONS

Figure 1 The invariant differential cross section for inclusive π^0 production in $\bar{p}p$ at $\sqrt{s}$ = 24.3 GeV.

Figure 2 η/π ratio as a function of p_T for pp and $\bar{p}p$ interactions.

Figure 3 The invariant differential cross section for direct photon production in $\bar{p}p$ interactions at $\sqrt{s}$ = 24.3 GeV. The dashed and solid lines are various theoretical predictions.

Figure 4 a) The differential cross sections as a function of |t| for pp and $\bar{p}p$ interactions at $\sqrt{s}$ = 24.3 GeV.

b) Comparison of the UA6 results (open circles) to measurements of ρ (pp) and ρ ($\bar{p}p$) at other energies.

Figure 5 a) J/ψ signal from our pp and $\bar{p}p$ data.

b) Comparison of $\bar{p}p$ cross sections time the branching ratio into e^+e^- inclusive production in the forward hemishere versus

$\sqrt{\tau}=M_{J/\psi} / \sqrt{s}$

c) Comparison of pp cross sections time the branching ratio into e^+e^- inclusive production in the forward hemishere versus

$\sqrt{\tau}=M_{J/\psi} / \sqrt{s}$

Figure 6 A schematic representation of single particle production with a polarized target.

Figure 7 The single spin asymmetry in π^+ and π^- production [12].

Figure 8 The single spin asymmetry in π^0 production measured with protons of 24 GeV/c incident momentum [13].

Figure 9 The single spin asymmetry in π^0 production measured with a negative pion beam of 40 GeV/c momentum [14].

Figure 10 The single spin asymmetry as a function of x in π^0 production measured with an antiproton beam of 40 GeV/c [15].

Figure 11 The polarized atomic hydrogen beam target.

Figure 12 Layout of the UA6 experiment in the SPS tunnel.

Figure 13 Breit-Rabi diagram of hydrogen atom ground state from ref. [34]. The energy W is given in units of $\Delta W = h \times 1420.4$ MHz$=5.8\ 10^{-6}$ eV, the magnetic field in units of $B_C=\Delta W/(g_I-g_j)\mu_B=507$ G, with g_I and g_j the proton and the electron g-factor and μ_B the Bohr magneton.

Figure 14 Schematic diagram of the polarized atomic hydrogen beam target.

Figure 15 Possible layout of the new trigger scintillators whithin the calorimeter.

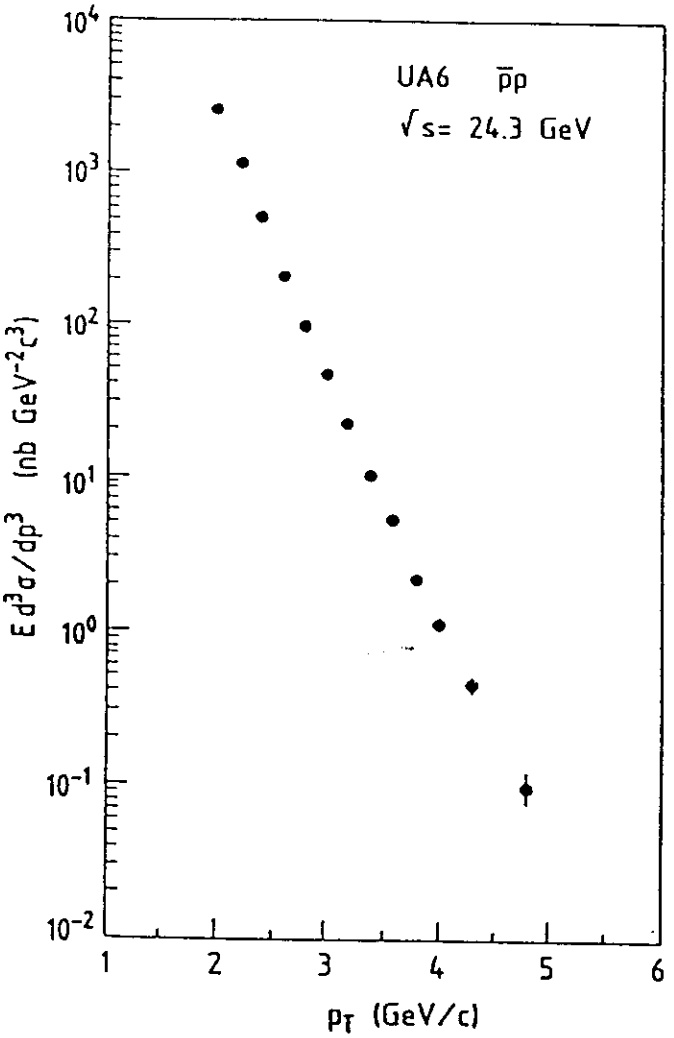
UA6 $\bar{p}p$
$\sqrt{s}$= 24.3 GeV
$E\,d^3\sigma/dp^3$ (nb GeV$^{-2}c^3$)
p_T (GeV/c)

Fig. 1

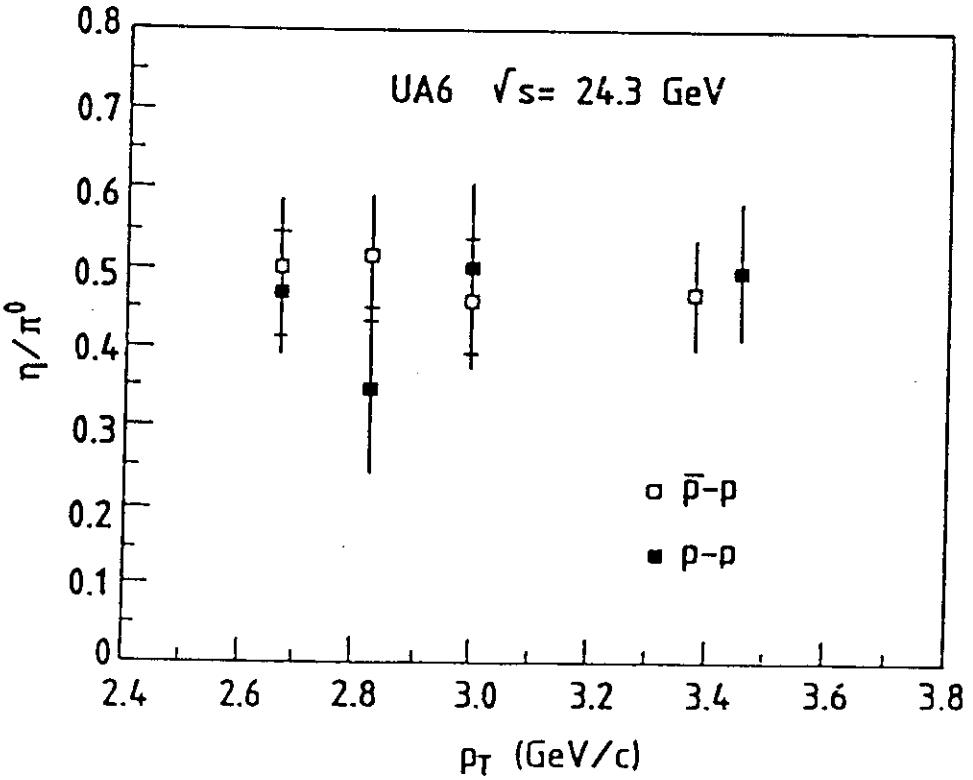
UA6 $\sqrt{s}$= 24.3 GeV
η/π^0
$\bar{p}$-p
p-p
p_T (GeV/c)

Fig. 2

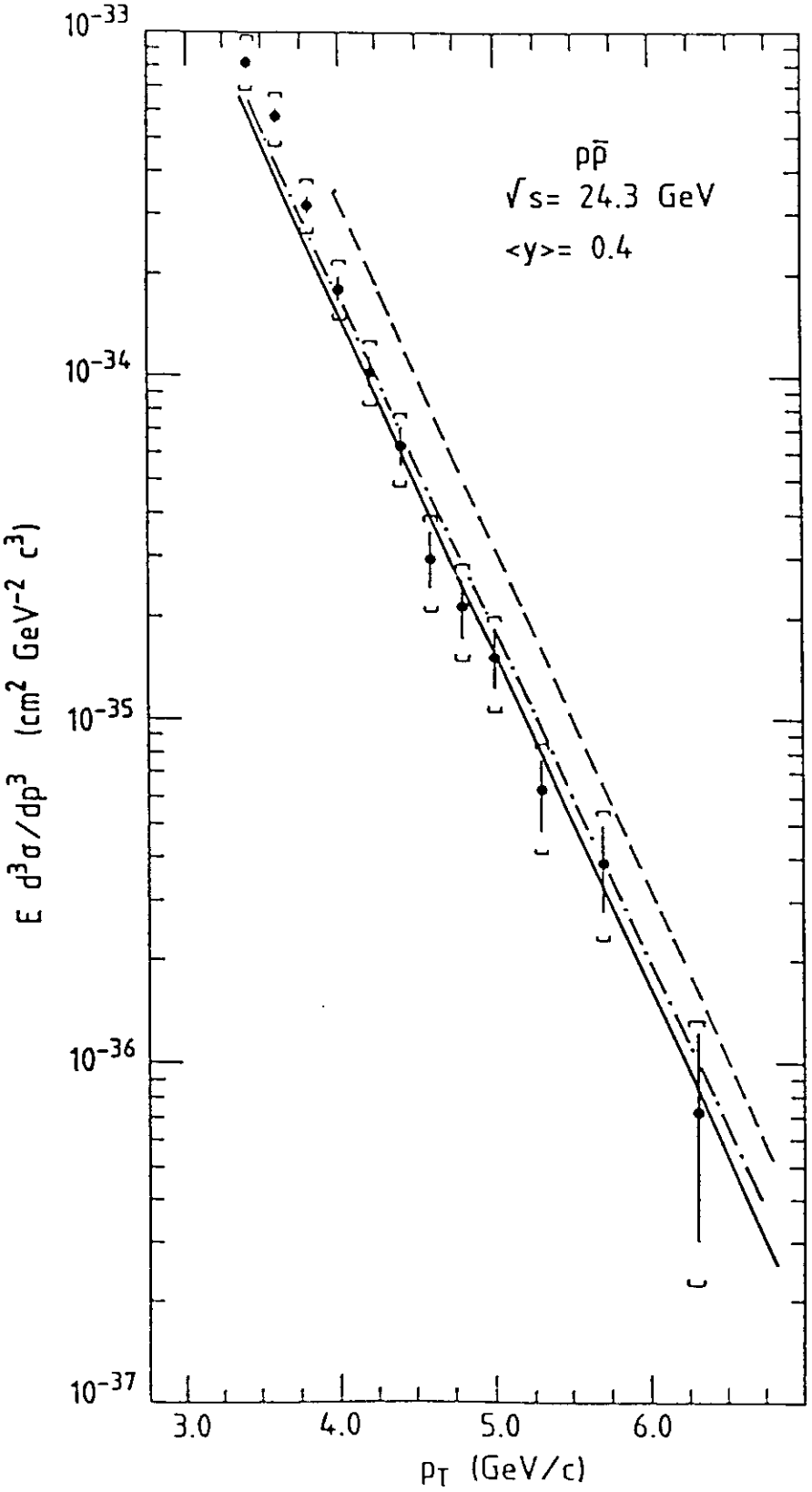
10^{-33}
10^{-34}
10^{-35}
10^{-36}
10^{-37}
$p\bar{p}$
$\sqrt{s}$= 24.3 GeV
<y>= 0.4
E $d^3\sigma/dp^3$ (cm^2 GeV^{-2} c^3)
3.0
4.0
5.0
6.0
p_T (GeV/c)

Fig. 3

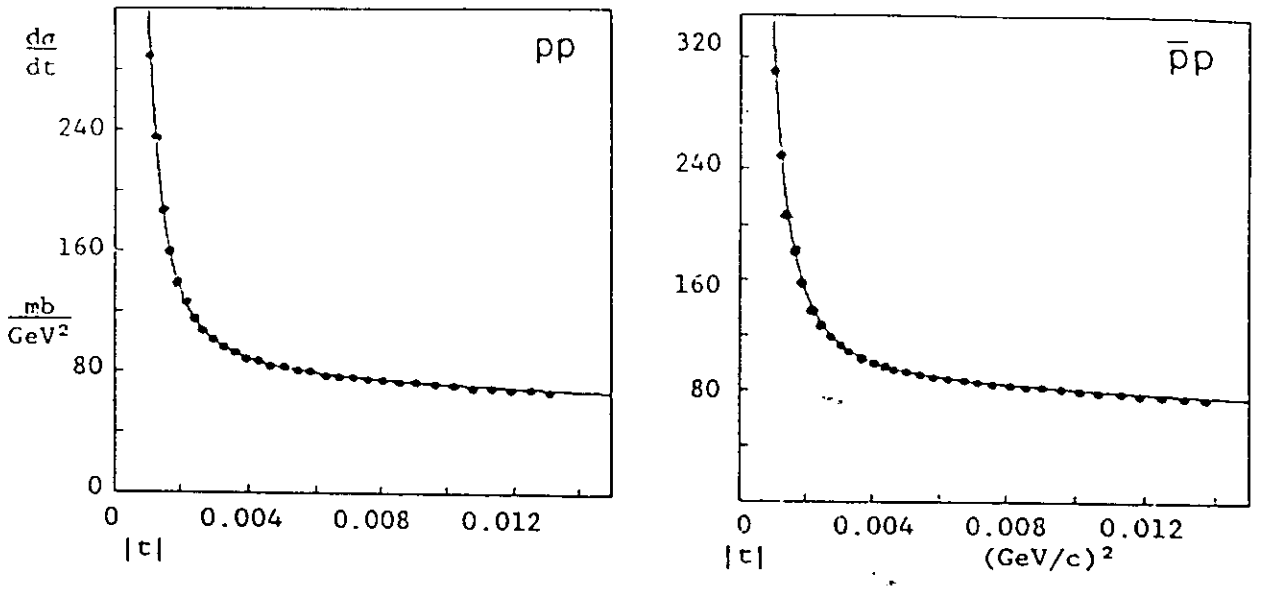
dσ/dt
pp
240
160
mb/GeV²
80
0
0
0.004
0.008
0.012
|t|
p̄p
320
240
160
80
0
0.004
0.008
0.012
|t|
(GeV/c)²

Fig.4a

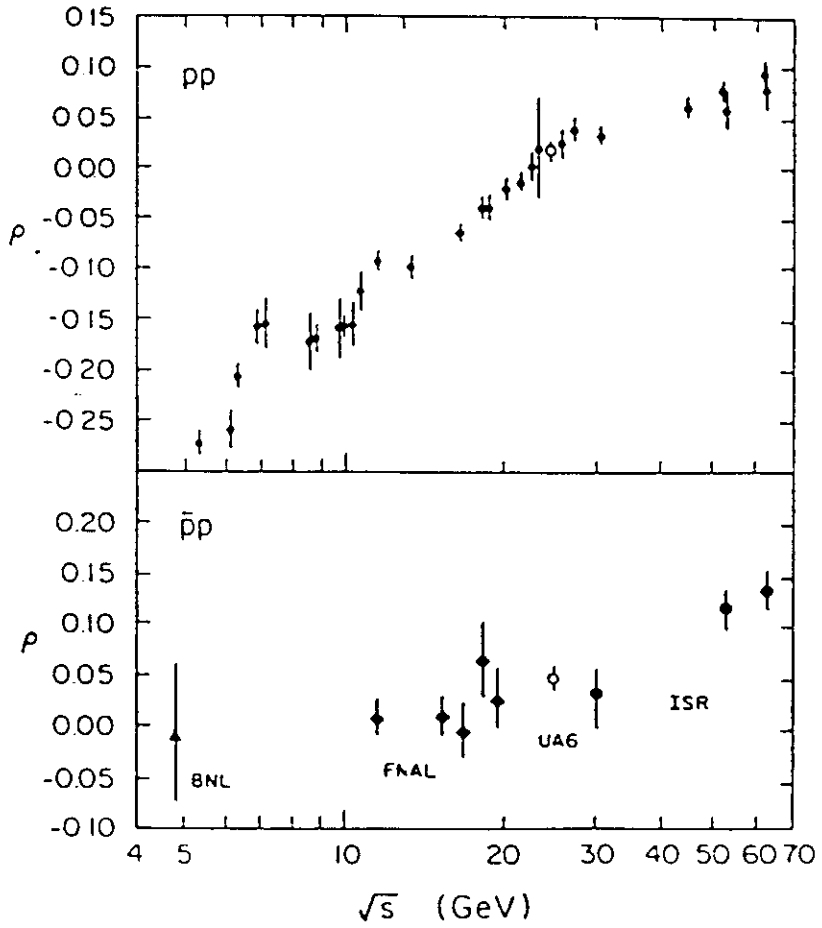
pp
p̄p
ρ
0.15
0.10
0.05
0.00
-0.05
-0.10
-0.15
-0.20
-0.25
0.20
0.15
0.10
0.05
0.00
-0.05
-0.10
BNL
FNAL
UA6
ISR
4
5
10
20
30
40
50
60
70
√s (GeV)

Fig. 4b

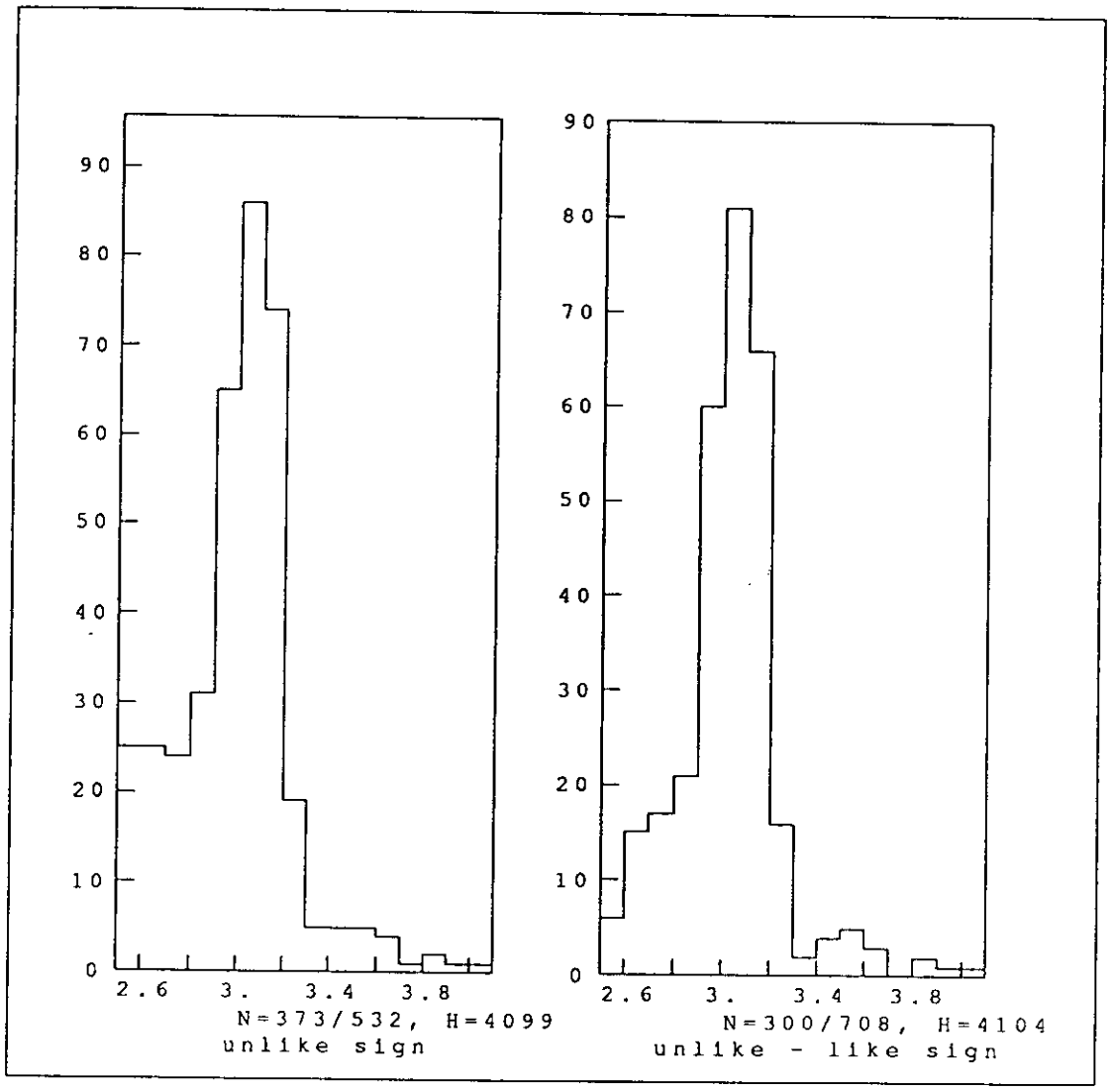
90
80
70
60
50
40
30
20
10
0
2.6
3.
3.4
3.8
N=373/532, H=4099
unlike sign
90
80
70
60
50
40
30
20
10
0
2.6
3.
3.4
3.8
N=300/708, H=4104
unlike - like sign

Fig . 5a

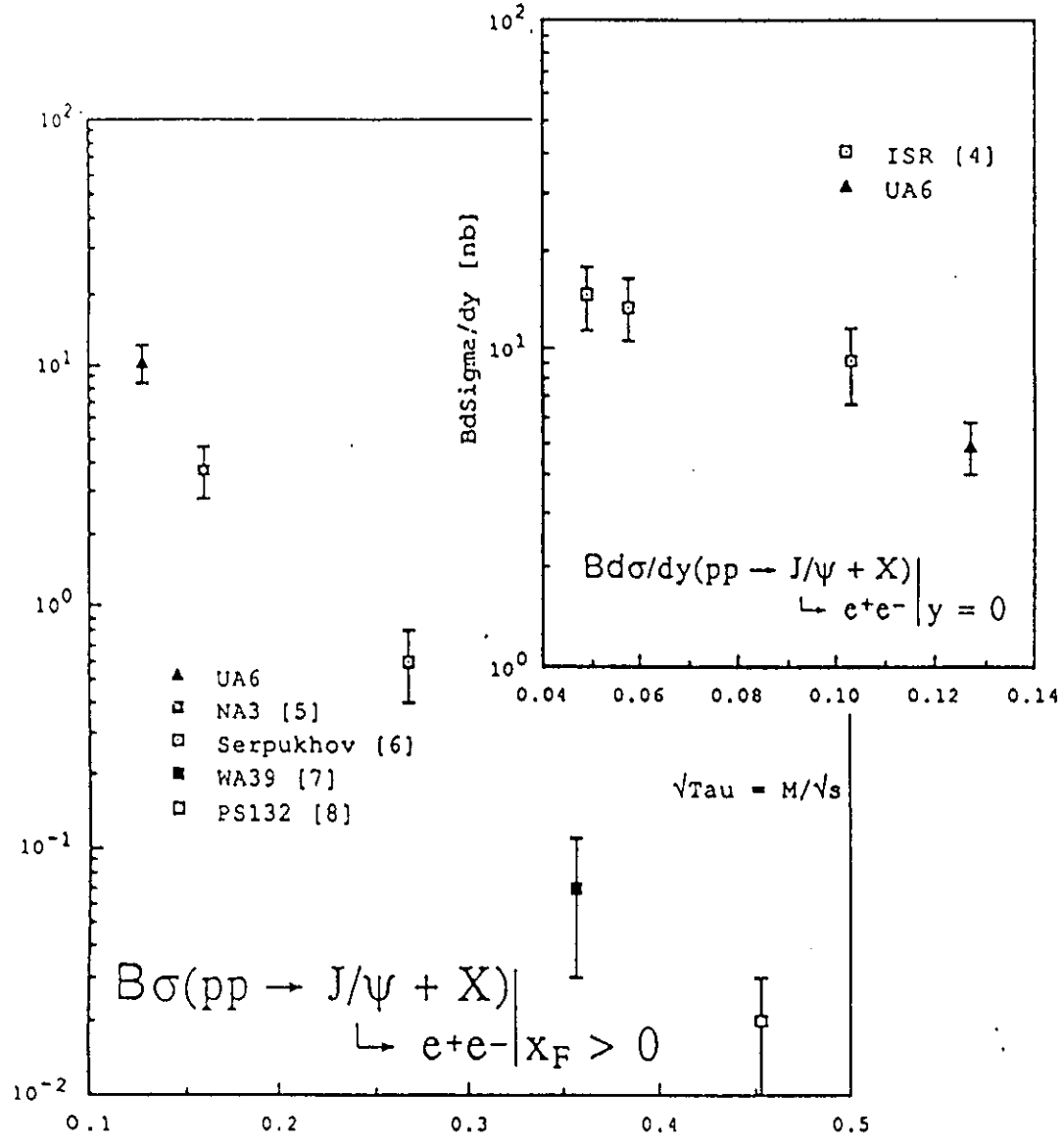
BdSigma/dy [nb]
ISR [4]
UA6
Bdσ/dy(pp → J/ψ + X)|↳ e+e-|y = 0
UA6
NA3 [5]
Serpukhov [6]
WA39 [7]
PS132 [8]
√Tau = M/√s
Bσ(pp → J/ψ + X)|↳ e+e-|xF > 0
√Tau = M/√s

Fig . 5b

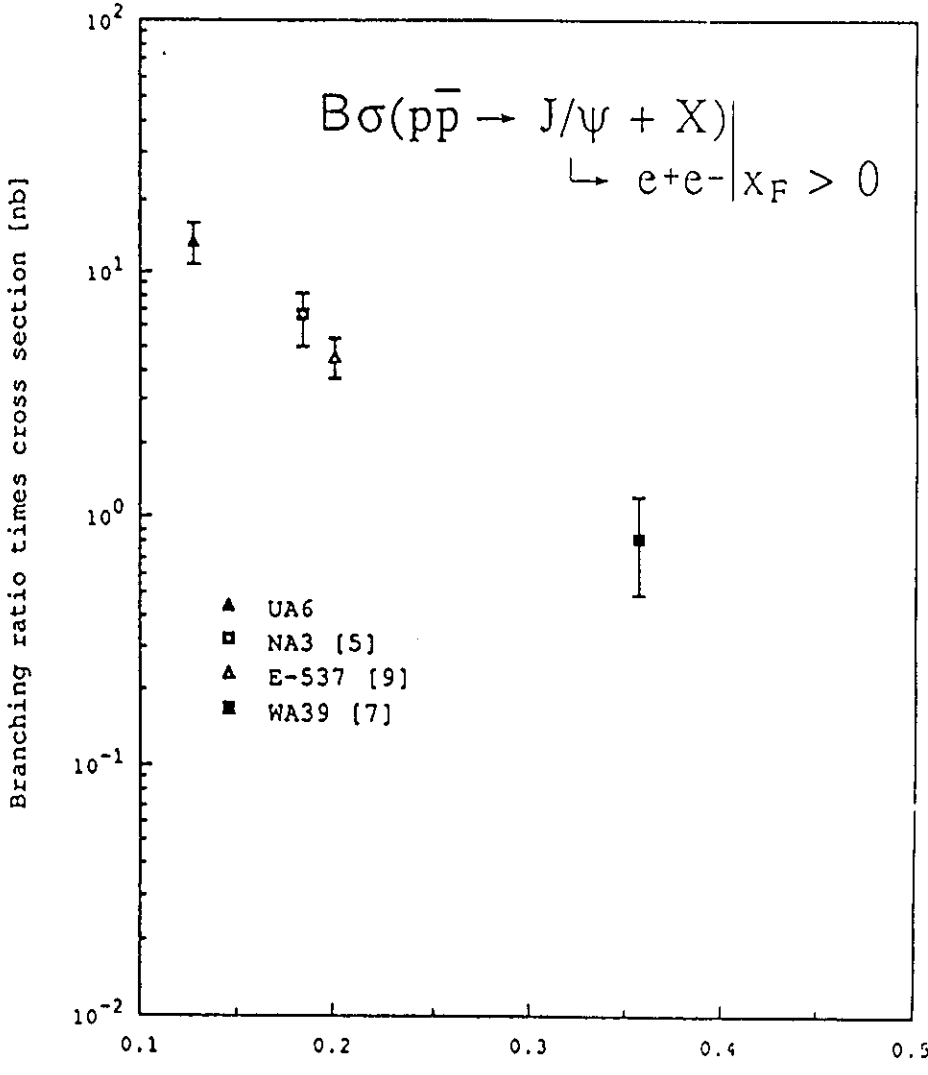
Branching ratio times cross section [nb]
Bσ(pp̄ → J/ψ + X)|↳ e+e-|xF > 0
UA6
NA3 [5]
E-537 [9]
WA39 [7]
√Tau = M/√s

Fig . 5c

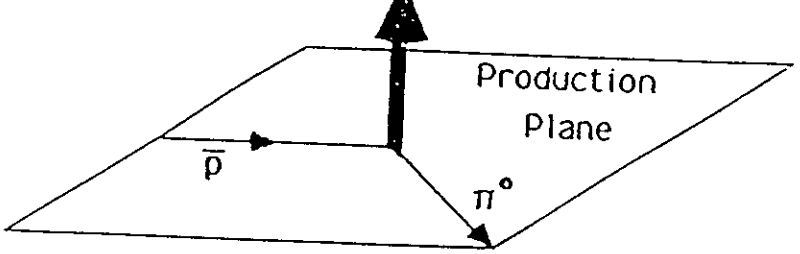
Production
Plane
$\bar{p}$
π^0

Fig.6

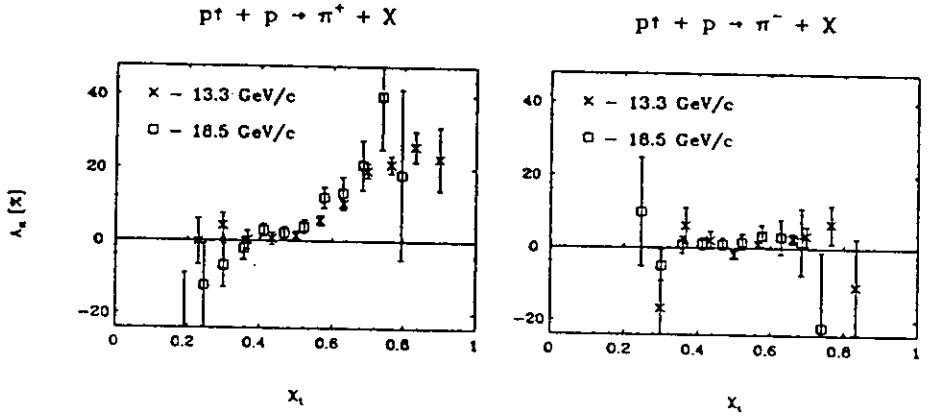
$p^\uparrow + p \to \pi^+ + X$
$p^\uparrow + p \to \pi^- + X$
× – 13.3 GeV/c
□ – 18.5 GeV/c
$A_N(x)$
x_F

Fig.7

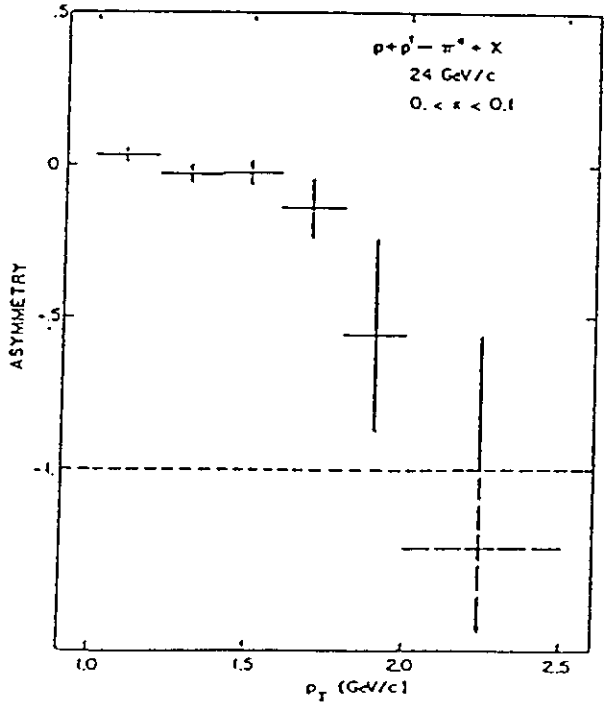
$p+p^\uparrow \to \pi^0 + X$
24 GeV/c
$0. < x < 0.1$
ASYMMETRY
p_T (GeV/c)

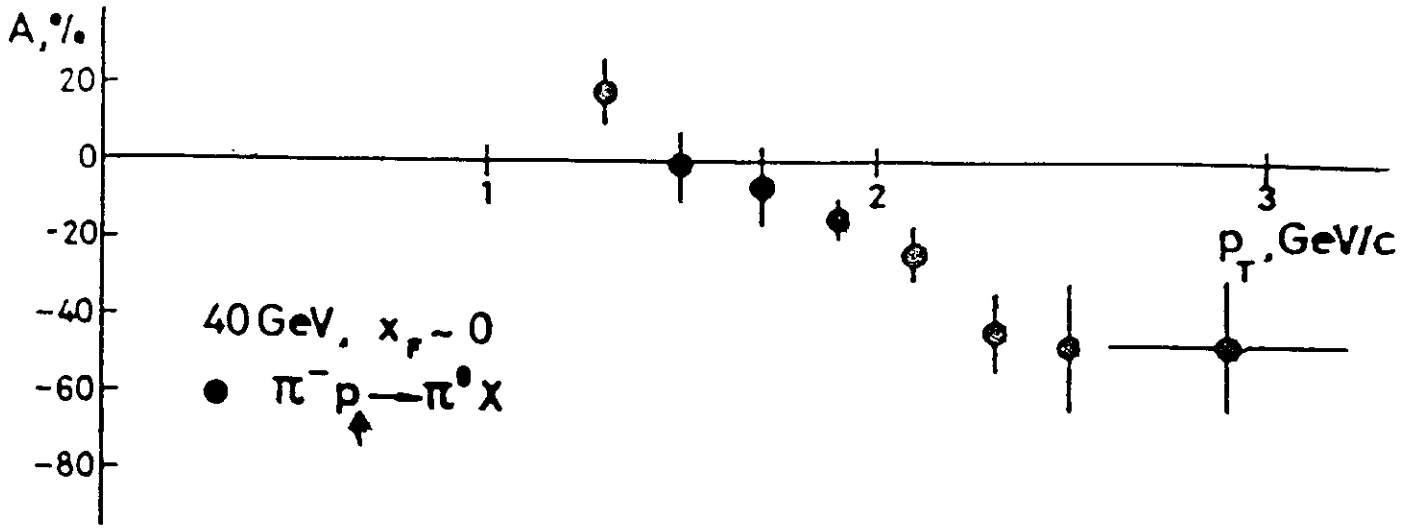
A, %
20
0
-20
-40
-60
-80
1
2
3
p_T, GeV/c
40 GeV, $x_F \sim 0$
$\pi^- p \rightarrow \pi^0 X$

Fig.9

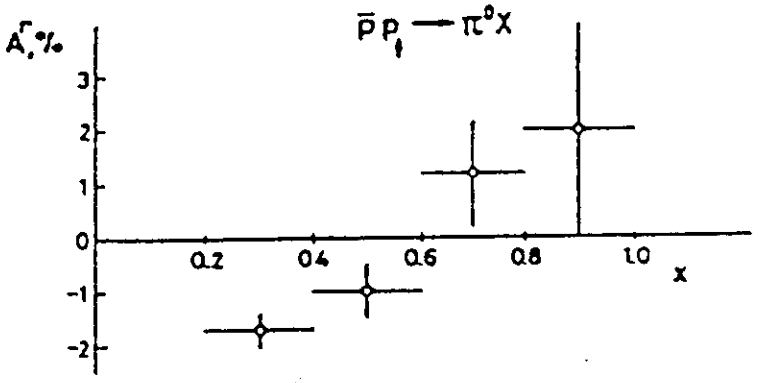
A_N, %
$\bar{p} p_\uparrow \rightarrow \pi^0 X$
3
2
1
0
-1
-2
0.2
0.4
0.6
0.8
1.0
x

Fig.10

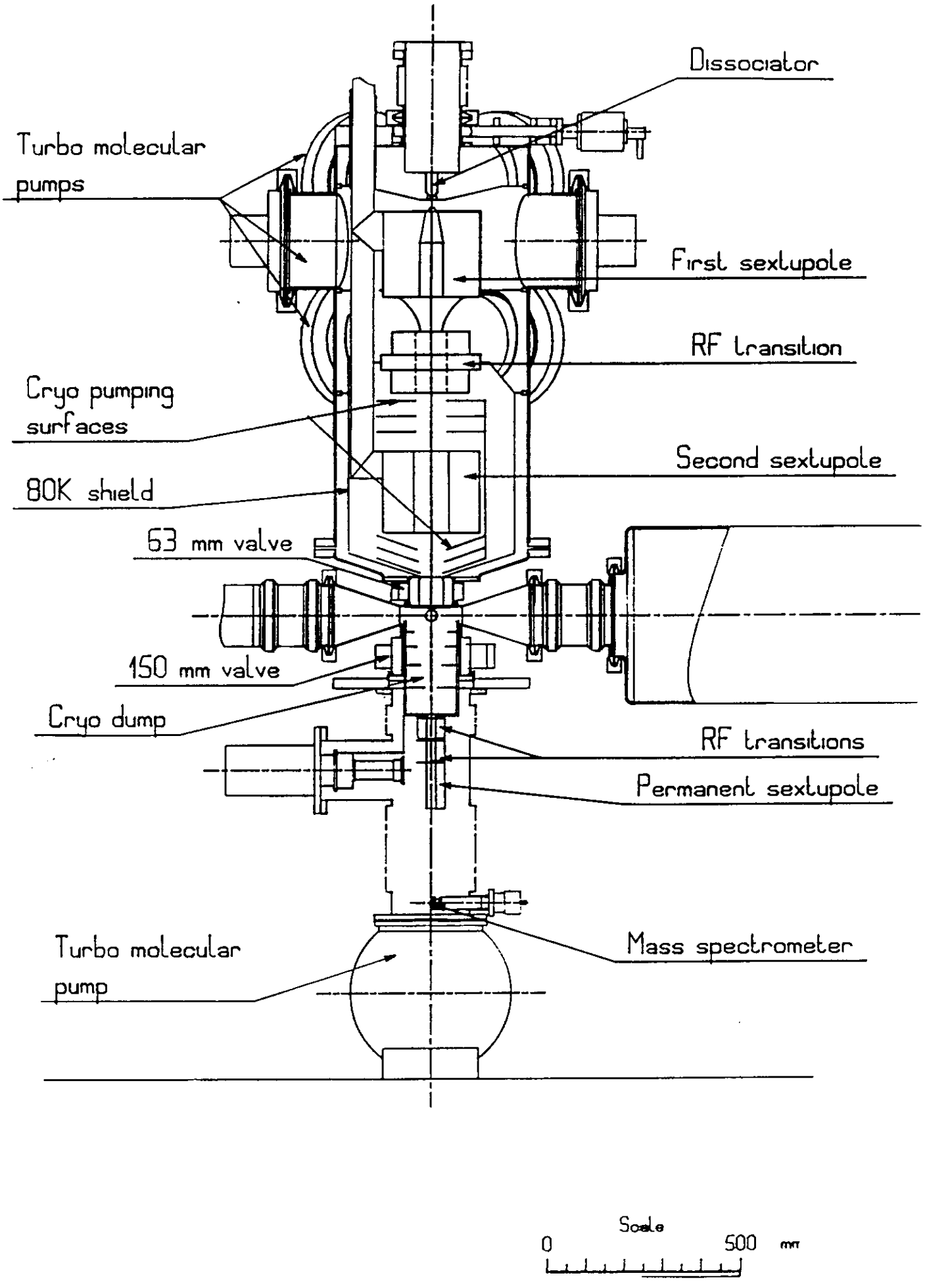
Dissociator
Turbo molecular pumps
First sextupole
RF transition
Cryo pumping surfaces
Second sextupole
80K shield
63 mm valve
150 mm valve
Cryo dump
RF transitions
Permanent sextupole
Turbo molecular pump
Mass spectrometer
Scale
0
500
mm

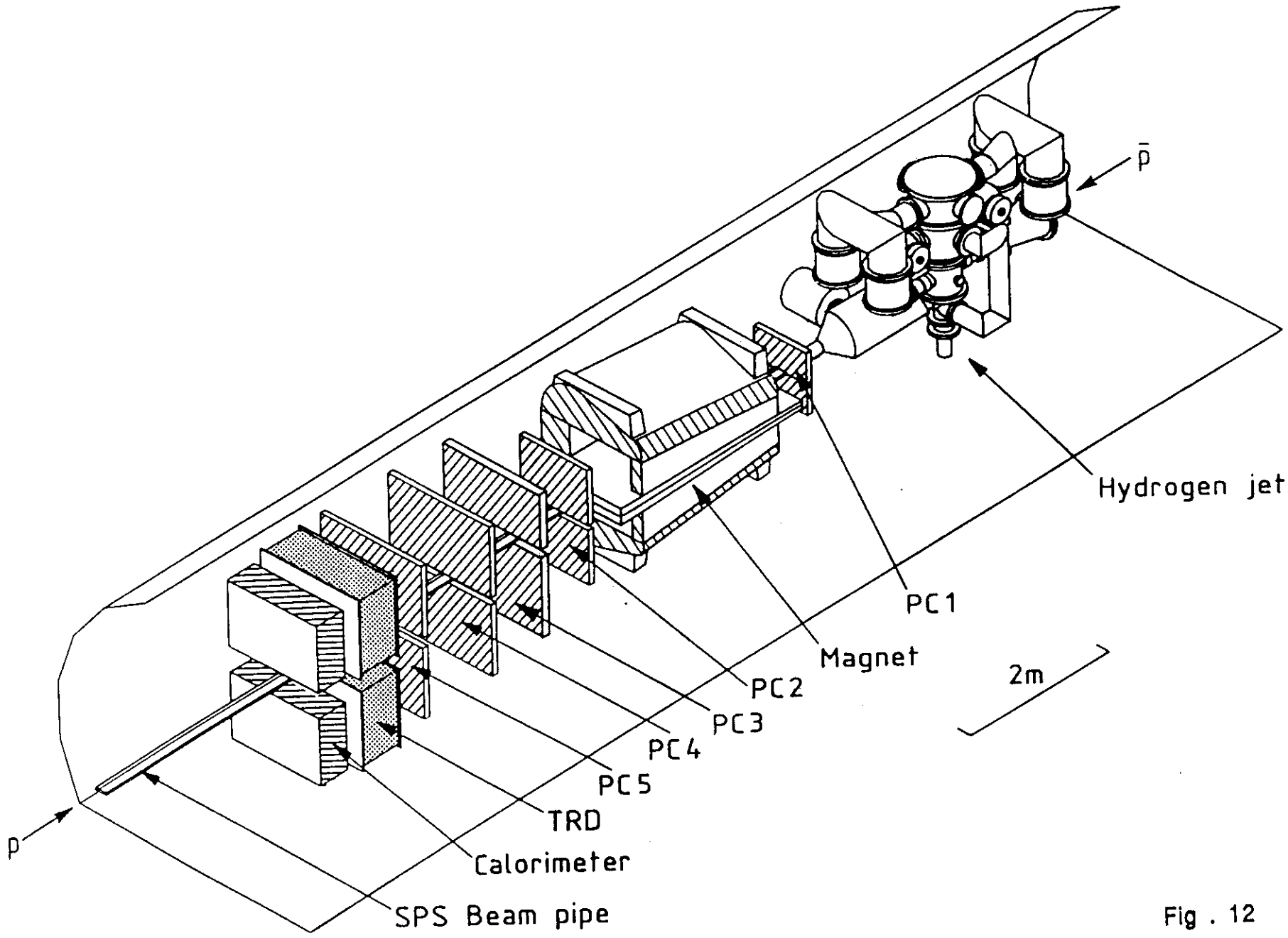
$\bar{p}$
Hydrogen jet
PC1
Magnet
PC2
PC3
PC4
PC5
TRD
Calorimeter
SPS Beam pipe
p
2m

Fig . 12

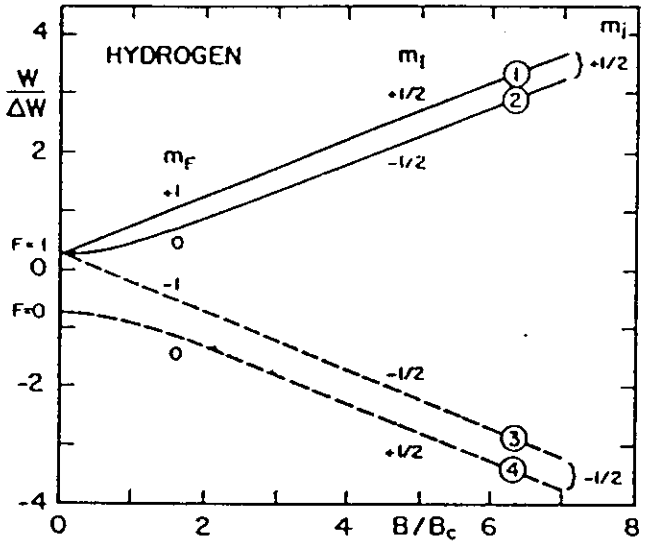
HYDROGEN
W/ΔW
B/B_c
m_j
m_I
m_F
+1/2
-1/2
+1
0
-1
F=1
F=0
1
2
3
4

Fig . 13

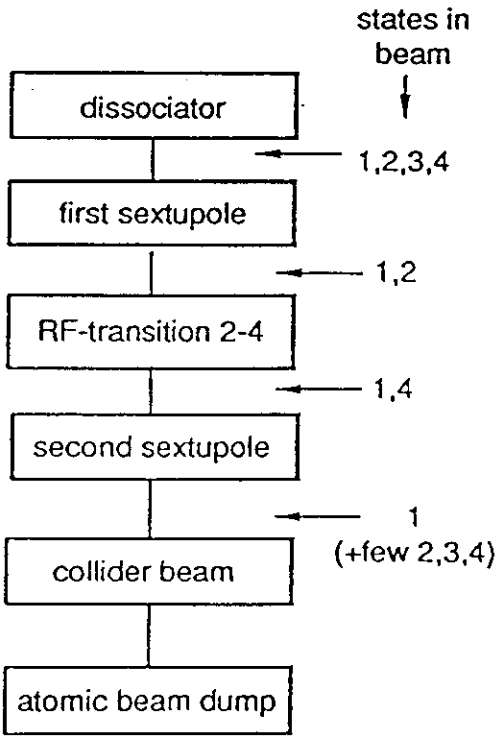
states in beam
dissociator
1,2,3,4
first sextupole
1,2
RF-transition 2-4
1,4
second sextupole
1
(+few 2,3,4)
collider beam
atomic beam dump

Fig . 14

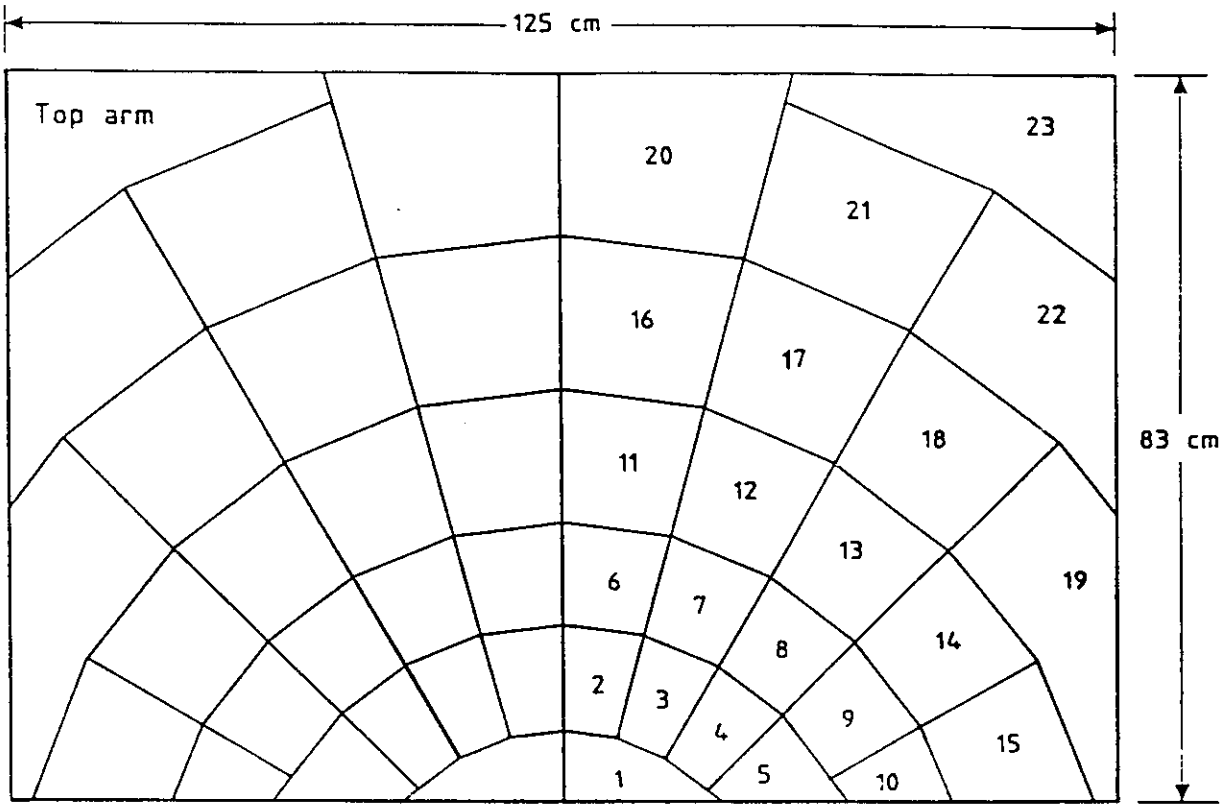
125 cm
Top arm
20
23
21
22
16
17
18
11
12
13
19
6
7
8
14
2
3
4
9
15
1
5
10
83 cm
⊗ Beam
Bottom arm

Figure 15